IOPscience iopscience.iop.org

Home Search Collections Journals About Contact us My IOPscience

Numerical solution of an inverse medium scattering problem with a stochastic source

This article has been downloaded from IOPscience. Please scroll down to see the full text article.

2010 Inverse Problems 26 074014

(http://iopscience.iop.org/0266-5611/26/7/074014)

View the table of contents for this issue, or go to the journal homepage for more

Download details:
IP Address: 128.211.160.44
The article was downloaded on 23/02/2012 at 19:55

Please note that terms and conditions apply.

Inverse Problems **26** (2010) 074014 (23pp) doi:10.1088/0266-5611/26/7/074014

Numerical solution of an inverse medium scattering problem with a stochastic source

Gang Bao[1,2], Shui-Nee Chow[3], Peijun Li[4] and Haomin Zhou[5]

[1] Department of Mathematics, Zhejiang University, Hangzhou 310027, People's Republic of China
[2] Department of Mathematics, Michigan State University, East Lansing, MI 48824, USA
[3] School of Mathematics, Georgia Institute of Technology, Atlanta, GA 30332, USA
[4] Department of Mathematics, Purdue University, West Lafayette, IN 47907, USA
[5] School of Mathematics, Georgia Institute of Technology, Atlanta, GA 30332, USA

E-mail: bao@math.msu.edu, chow@math.gatech.edu, lipeijun@math.purdue.edu and hmzhou@math.gatech.edu

Received 31 December 2009, in final form 11 May 2010
Published 1 July 2010
Online at stacks.iop.org/IP/26/074014

Abstract

This paper is concerned with the inverse medium scattering problem with a stochastic source, the reconstruction of the refractive index of an inhomogeneous medium from the boundary measurements of the scattered field. As an inverse problem, there are two major difficulties in addition to being highly nonlinear: the ill-posedness and the presence of many local minima. To overcome these difficulties, a stable and efficient recursive linearization method has been recently developed for solving the inverse medium scattering problem with a deterministic source. Compared to classical inverse problems, stochastic inverse problems, referred to as inverse problems involving uncertainties, have substantially more difficulties due to randomness and uncertainties. Based on the Wiener chaos expansion, the stochastic problem is converted into a set of decoupled deterministic problems. The strategy developed is a new hybrid method combining the WCE with the recursive linearization method for solving the inverse medium problem with a stochastic source. Numerical experiments are reported to demonstrate the effectiveness of the proposed approach.

(Some figures in this article are in colour only in the electronic version)

1. Introduction

Motivated by significant scientific and industrial applications, the field of inverse problems has undergone a tremendous growth in the last several decades. There are a variety of inverse problems, including identification of partial differential equation coefficients, reconstruction of

 © 2010 IOP Publishing Ltd Printed in the UK & the USA

initial data, estimation of source functions and detection of interfaces or boundary conditions. Scattering problems are concerned with the effect an inhomogeneous medium has on an incident wave [29]. In particular, if the total field is viewed as the sum of an incident field and a scattered field, the direct scattering problem is to determine the scattered field from a knowledge of the incident field and the medium; the inverse scattering problem is to determine the nature of the inhomogeneity from knowledge of the scattered field [30]. Inverse scattering problems are basic in many scientific areas such as radar and sonar, geophysical exploration, medical imaging and near-field optics imaging [31].

This paper is concerned with the inverse medium scattering problem, i.e. the reconstruction of the refractive index of an inhomogeneous medium from scattering data. In addition to being highly nonlinear, there are two major difficulties associated with the inverse problem: the ill-posedness and the presence of many local minima. A number of algorithms have been proposed for numerical solutions of this inverse problem, e.g. [1, 19, 33, 35–37, 43, 44, 49, 50] and references cited therein. Classical iterative optimization methods offer fast local convergence but often fail to compute the global minimizers because of multiple local minima. Another main difficulty is the ill-posedness, i.e. infinitesimal noise in the measured data may give rise to a large error in the computed solution. It is well known that the ill-posedness of the inverse scattering problem decreases as the frequency increases. However, at high frequencies, the nonlinear equation becomes extremely oscillatory and possesses many more local minima. A challenge for solving the inverse problem is to develop solution methods that take advantage of the regularity of the problem for high frequencies without being undermined by local minima.

To overcome the difficulties, stable and efficient recursive linearization methods (RLM) have been developed for solving the two-dimensional Helmholtz equation and the three-dimensional Maxwell's equations in the case of full aperture data [6, 8, 20] and in limited aperture data cases [5, 9, 10, 12]. In the case of fixed frequencies, a related continuation approach has been developed on the spatial frequencies [7, 11, 21]. A recursive linearization approach has also been developed for solving inverse obstacle problems by Coifman *et al* [26]. More recently, direct imaging techniques have been explored to replace the weak scattering for generating the initial guess [4]. We refer readers to [13] for the mathematical analysis of the general recursive linearization algorithm for solving inverse medium problems with multi-frequency measurements. Roughly speaking, these methods use the Born approximation at the lowest frequency to obtain initial guesses which are the low-frequency modes of the medium. Updates are made by using the data at higher frequencies sequentially until a sufficiently high frequency where the dominant modes of the medium are essentially recovered. The underlying physics which permits the successive recovery is the so-called Heisenberg uncertainty principle: it is increasingly difficult to determine features of the scatterer as its size becomes decreasingly smaller than half of a wavelength. One may consult Colton *et al* [28] and Natterer [42] for a recent account of general inverse scattering problems.

Stochastic inverse problems refer to the inverse problems that involve uncertainties, which are widely introduced to the mathematical models for three major reasons: (1) randomness directly appears in the studied systems; (2) incomplete knowledge of the systems must be modeled by uncertainties; (3) stochastic techniques are introduced to couple the interference between different scales more effectively, especially when the scale span is large. The first two reasons are commonly encountered and they can happen simultaneously for many different problems. It is only recently that the third one has started being recognized as an effective tool for handling long-range multiscale problems. It is our intention to study inverse scattering with randomness and uncertainties entering the problem because of all the reasons mentioned. Compared to deterministic inverse problems, stochastic inverse problems have substantially more difficulties on top of the existing hurdles, mainly due to randomness and

uncertainties. For instance, unlike the deterministic nature of solutions for classical inverse problems, the solution for a stochastic inverse problem is random functions. Therefore, it is less meaningful to find a solution for a particular realization of the randomness. The popular Monte Carlo simulations to compute the statistics often demand several orders more computational resources over the corresponding classical inverse problems. For these reasons, new models and methodologies are highly desired in related applications.

In this work, we study the inverse medium problem with a spatially stochastic source, where the medium itself is deterministic but the source function is modeled as a stochastic function. The random source problem for wave propagation has been considered as a basic tool for the solution of reflection tomography, diffusion-based optical tomography and more recently fluorescence microscopy [52], which allows systematic imaging studies of protein localization in living cells and of the structure and function of living tissues. The fluorescence in the specimen (such as green fluorescent protein) gives rise to emitted light which is focused to the detector by the same objective that is used for the excitation. Mathematically, it will be more appropriate to describe the source as a stochastic function due to its small scale and random nature. We refer to [3, 32] for related inverse random source problems, and [25, 39, 40, 46] for wave propagation in random media.

In solving classical deterministic inverse problems, it is a common feature in the existing strategies that the associated direct problems must be solved multiple times. Therefore, it is important to develop models and efficient methods for the stochastic direct problems. To tackle the problem, we employ the Wiener chaos expansion (WCE)-based approach, which is a classical orthonormal expansion theory for random functions that was first introduced by Cameron and Martin [18]. The WCE theory is based on the fact that Hermite polynomials are orthonormal polynomials of Gaussian random variables. If the random variables have different distribution other than Gaussian, the theory is still true except that one has to replace Hermite polynomials by different series of polynomials that are orthonormal with respect to the distributions. In that case, the theory is called generalized polynomial chaos expansion, see [51] for more references on WCE and related subjects. Recently, a novel and efficient WCE-based technique has been developed for modeling and simulation of spatially incoherent sources in photonic crystals by Badieirostami *et al* [2]. The basic idea is that the incoherent source can be modeled by a stochastic process, which leads to a partial differential equation with a stochastic source. According to WCE theory, the random source term has an expansion under some orthonormal basis functions. By substituting the expression into the stochastic equation, a set of deterministic differential equations can be obtained with new deterministic source terms. The stochastic problem can thus be converted into a set of decoupled deterministic problems. To solve the inverse medium scattering problem with a stochastic source, we develop a hybrid method of combining the novel WCE-based model with the RLM. This combination forms a new iterative procedure and provides useful techniques to handle the randomness and uncertainties arising from the stochastic inverse problem. The work represents our initial attempt towards more complex model problems.

Though the stochastic equation can be converted into a set of deterministic equations, they are imposed in an open domain. To apply numerical methods, the open domain needs to be truncated into a bounded domain. A suitable boundary condition has to be imposed on the boundary of the bounded domain so that no artificial wave reflection occurs. We use the uniaxial perfectly matched layer (PML) technique to truncate the open domain. The PML technique, which was first proposed by Berenger [15, 16], is an important and popular mesh termination technique in computational wave propagation due to its effectiveness, simplicity and flexibility, e.g. [47, 48]. Under the assumption that the exterior solution is composed of outgoing waves only, the basic idea of the PML technique is to surround the computational

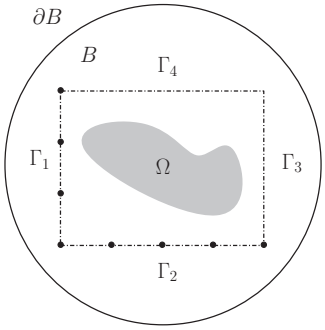

Figure 1. Geometry of the scattering problem with a transparent boundary.

domain by a layer of finite thickness with specially designed model medium that would either slow down or attenuate all the waves that propagate from inside the computational domain. It has been proved that the PML solution can converge exponentially to the solution of the original scattering problem as the thickness of the PML layer or the medium parameters tend to infinite, see e.g. [14, 17, 23, 24, 27, 41].

The outline of the paper is as follows. In section 2, a stochastic forward problem is introduced; based on WCE theory, the stochastic model is converted into a set of deterministic model problems; energy estimates of the wave fields are obtained; a PML formulation is presented to reduce the model problem into a bounded domain. Section 3 is devoted to the introduction of the RLM for the inverse medium problem. To regularize the RLM, regularization functionals are provided from the optimization point of view. An algorithm of the hybrid method of combining WCE with RLM is described. In section 4, we discuss numerical implementation of the hybrid method and present three numerical examples to demonstrate the effectiveness of the proposed approach. The paper is concluded with general remarks and directions for future research in section 5.

2. Direct scattering problem

In this section, we introduce the two-dimensional Helmholtz equation with a stochastic source as a model problem. Based on the WCE theory, we convert the stochastic problem into a set of deterministic problems. After reducing the problem imposed in the open domain into one in a bounded domain using the Dirichet-to-Neumann (DtN) operator, we discuss a variational formulation of the direct problem and present some energy estimates for the wave fields. To apply numerical methods, the uniaxial PML technique is introduced to truncate the open domain into a bounded rectangular domain.

2.1. A model problem

Deducing from the system of time-harmonic Maxwell's equations, we consider the two-dimensional Helmholtz equation

$$\Delta u + \omega^2(1+q)u = \mathrm{i}\omega f \quad \text{in} \quad \mathbb{R}^2, \tag{2.1}$$

where ω is the angular frequency, $q > -1$ is the scatterer which is assumed to have a compact support contained in a rectangular domain Ω with four side boundaries Γ_j, $j = 1, \ldots, 4$, as seen in figure 1, and the current density f is the source of excitation and is modeled as

two one-dimensional arrays of spatially incoherent point sources along the line segments Γ_1 and Γ_2.

For modeling the spatially incoherent source, any two point source on the line segments Γ_1 or Γ_2 should radiate independently of each other. This definition by itself can be used as the brute-force technique for numerical modeling of the spatially incoherent source. In such modeling, zero correlation is enforced between the contributions from every two input point sources on the line segments Γ_1 and Γ_2 by separately analyzing the structure with each point source and adding the individual contributions at the output incoherently. While this technique perfectly describes the incoherent source, it is very time consuming practically since it requires one simulation of the entire structure for each input point source.

To reduce the simulation time, we adopt the WCE-based technique, which is proposed by Badieirostami *et al* [2]. To model the spatially incoherent source, white noise is used, i.e. the derivative of the Brownian motion, to model the current density f. More precisely, we represent the spatially incoherent source along two segment lines at Γ_1 and Γ_2 as

$$f(x, y) = \mathrm{d}W(x, y), \tag{2.2}$$

where $\mathrm{d}W(x, y)$ is the derivative of the Brownian motion representing the independent spatial randomness along x and y. According to WCE theorem, by choosing any orthonormal basis function $\{\phi_i(x), \psi_j(y)\}$, $i, j = 1, 2, \ldots$, in the rectangular domain Ω, we can introduce a set of independent standard Gaussian random variables $\{\xi_{ij}\}$ such that

$$\mathrm{d}W(x, y) = \sum_{i,j} \xi_{ij}\phi_i(x)\psi_j(y)$$

with

$$\xi_{ij} = \int_\Omega \phi_i(x)\psi_j(y)\,\mathrm{d}W(x, y).$$

In practice, we choose a set of sinusoidal basis functions for $\phi_i(x)$ and $\psi_j(y)$ given by Hou *et al* [38]:

$$\psi_1(y) = \frac{1}{\sqrt{|\Gamma_1|}}, \qquad \psi_j(y) = \sqrt{\frac{2}{|\Gamma_1|}}\cos\left[(j-1)\pi\frac{y}{|\Gamma_1|}\right], \qquad j = 2, \ldots,$$

$$\phi_1(x) = \frac{1}{\sqrt{|\Gamma_2|}}, \qquad \phi_i(x) = \sqrt{\frac{2}{|\Gamma_2|}}\cos\left[(i-1)\pi\frac{x}{|\Gamma_2|}\right], \qquad i = 2, \ldots,$$

where $|\Gamma_1|$ and $|\Gamma_2|$ are the lengths of the line segments Γ_1 and Γ_2, respectively.

The WCE method separates the deterministic effects from randomness. Therefore, the original stochastic Helmholtz equation is reduced into an associated set of deterministic equations for the expansion coefficients. Using the formulation described above, we deduce the following set of deterministic equations for the expansion coefficients (dropping the subscript for clarity):

$$\Delta u + \omega^2(1+q)u = \mathrm{i}\omega\varphi, \tag{2.3}$$

where

$$\varphi(x, y) = \phi(x)\psi(y).$$

In addition, the standard Sommerfeld radiation condition is imposed to ensure the uniqueness of the solution. Therefore, we need to simulate the structure for each basis function ϕ and ψ to find the corresponding u defined in equation (2.3).

The source function is modeled as the derivative of the Brownian motion, i.e. white noise, which is a spatial Gaussian random field. The data will be assumed to be a spatial Gaussian

random field since the medium is assumed to be a deterministic function. Based on WCE, it is possible to decompose the random data into a sequence of deterministic components corresponding to the chosen orthonormal basis functions, which projects the data into the spaces spanned by each individual function in the set of orthornormal basis under the sense of taking expectation. According to the strong law of large numbers, the data with a large amount of realizations will be required to obtain a good approximation to the expectation value when doing the data decomposition. We admit that this step is absolutely nontrivial and involve much effort. It is an ongoing project to decompose the boundary measurements of the random wave field u according to the chosen orthonormal basis functions and we will report the progress somewhere else.

Remark 2.1. The inverse medium problem is to reconstruct the scatterer function q from the boundary measurement of the random wavefield u corresponding to the stochastic source f. According to WCE theory, we may assume that the boundary measurement of the deterministic wavefield component of u is known for each orthonormal basis function φ. Therefore, the boundary data will be taken as the wavefield u corresponding to the orthonormal basis function φ in the description of the reconstruction method.

Remark 2.2. The choice of the basis function will not change the structure of the algorithm, but it may have an impact on the efficiency and convergence rate of the reconstructions. We did not pursue the comparisons between different bases, which is actually an interesting problem to study in the future. Once the orthonormal basis functions are chosen, we should use them for both the direct and inverse problems as the data will be decomposed based on the chosen basis as well.

2.2. Analysis of the direct scattering

Using the DtN operator, we reduce equation (2.3) from the open domain into a bounded disk, study its variational formulation and present some energy estimates. The energy estimates provide the theoretical basis to generate initial guesses for the iterative RLM.

Let the support of the scatterer Ω be contained in the interior of the disk $B_R = \{\mathbf{x} \in \mathbb{R}^2 : |\mathbf{x}| < R\}$ with boundary $\partial B_R = \{\mathbf{x} \in \mathbb{R}^2 : |\mathbf{x}| = R\}$, as seen in figure 1. In the domain $\mathbb{R}^2 \setminus \bar{B}$, the solution of (2.3) can be written under the polar coordinates as follows:

$$u(\rho, \theta) = \sum_{n\in\mathbb{Z}} \frac{H_n^{(1)}(\omega\rho)}{H_n^{(1)}(\omega R)} \hat{u}_n \, \mathrm{e}^{\mathrm{i}n\theta}, \tag{2.4}$$

where

$$\hat{u}_n = \frac{1}{2\pi} \int_0^{2\pi} u(R, \theta) \, \mathrm{e}^{-\mathrm{i}n\theta} \, \mathrm{d}\theta,$$

and $H_n^{(1)}$ is the Hankel function of the first kind with order n. For any function u defined on the circle ∂B_R having the Fourier expansion:

$$u = \sum_{n\in\mathbb{Z}} \hat{u}_n \, \mathrm{e}^{\mathrm{i}n\theta} \qquad \text{with} \quad \hat{u}_n = \frac{1}{2\pi} \int_0^{2\pi} u \, \mathrm{e}^{-\mathrm{i}n\theta} \, \mathrm{d}\theta,$$

we define

$$\|u\|^2_{H^{1/2}(\partial B_R)} = 2\pi \sum_{n\in\mathbb{Z}} (1 + n^2)^{1/2} |\hat{u}_n|^2,$$

$$\|u\|^2_{H^{-1/2}(\partial B_R)} = 2\pi \sum_{n\in\mathbb{Z}} (1 + n^2)^{-1/2} |\hat{u}_n|^2.$$

Let $T : H^{1/2}(\partial B_R) \to H^{-1/2}(\partial B_R)$ be the DtN operator defined as follows: for any $u \in H^{1/2}(\partial B_R)$,

$$Tu = \frac{\omega}{R} \sum_{n\in\mathbb{Z}} \frac{H_n^{(1)'}(\omega R)}{H_n^{(1)}(\omega R)} \hat{u}_n \, \mathrm{e}^{\mathrm{i}n\theta}. \tag{2.5}$$

Using the DtN operator, the solution in (2.4) satisfies the following transparent boundary condition:

$$\partial_{\mathbf{n}} u = Tu \quad \text{on} \quad \partial B_R, \tag{2.6}$$

where $\mathbf{n}$ is the unit outward normal to ∂B_R.

To state the boundary value problem, we introduce the bilinear form $a : H^1(B_R) \times H^1(B_R) \to \mathbb{C}$

$$a(u, v) = (\nabla u, \nabla v) - \omega^2 ((1 + q)u, v) - \langle Tu, v\rangle, \tag{2.7}$$

and the linear functional on $H^1(B_R)$

$$b(v) = -\mathrm{i}\omega(\varphi, v). \tag{2.8}$$

Here we have used the standard inner products

$$(u, v) = \int_{B_R} u \cdot \bar{v} \qquad \text{and} \qquad \langle u, v\rangle = \int_{\partial B_R} u \cdot \bar{v},$$

where the bar denotes the complex conjugate. The direct problem (2.3) is equivalent to the following weak formulation. Find $u \in H^1(B_R)$ such that

$$a(u, v) = b(v) \qquad \text{for all} \quad u \in H^1(B_R). \tag{2.9}$$

Before presenting the main results for the variational problem, we state a useful lemma for the regularity of the DtN operator. Readers are referred to [45] for detailed discussions and proofs.

Lemma 2.1. *There exists a constant C such that for any $u \in H^{1/2}(\partial B_R)$ the following inequality holds:*

$$\|Tu\|_{H^{-1/2}(\partial B_R)} \leqslant C\|u\|_{H^{1/2}(\partial B_R)}.$$

Furthermore,

$$-\mathrm{Re}\langle Tu, u\rangle \geqslant C\|u\|^2_{L^2(\partial B_R)} \qquad \text{and} \qquad \mathrm{Im}\langle Tu, u\rangle \geqslant 0.$$

Next we prove the well-posedness of the variational problem (2.9) and obtain an energy estimate for the wave field with a uniform bound with respect to the frequency in the case of small frequencies.

Theorem 2.1. *If the frequency ω is sufficiently small, the variational problem (2.9) admits a unique weak solution in $H^1(B_R)$. Further, there is a positive constant C such that*

$$\|u\|_{H^1(B_R)} \leqslant C\omega\|\varphi\|_{L^2(B_R)}. \tag{2.10}$$

Proof. Decompose the bilinear form a into $a = a_1 - \omega^2 a_2$, where

$$a_1(u, v) = (\nabla u, \nabla v) - \langle Tu, v\rangle \qquad \text{and} \qquad a_2(u, v) = ((1 + q)u, v)\,.$$

We conclude that a_1 is coercive from lemma 2.1:

$$|a_1(u, u)| \geqslant C\|u\|^2_{H^1(B)}.$$

Next we prove the compactness of a_2. Define an operator $A : L^2(B) \to H^1(B)$ by

$$a_1(Au, v) = a_2(u, v) \qquad \text{for all} \quad v \in H^1(B),$$

which gives

$$(\nabla Au, \nabla v) - \langle TAu, v\rangle = ((1+q)u, v)\,.$$

Using the Lax–Milgram lemma and lemma 2.1, we obtain

$$\|Au\|_{H^1(B)} \leqslant C\|u\|_{L^2(B)}. \tag{2.11}$$

Thus, A is bounded from $L^2(B)$ to $H^1(B)$ and $H^1(B)$ is compactly embedded into $L^2(B)$. Hence, A is a compact operator.

Define a function $w \in L^2(B)$ by requiring $w \in H^1(B)$ and satisfying

$$a_1(w, v) = b(v) \qquad \text{for all} \quad v \in H^1(B).$$

It follows from the Lax–Milgram lemma again that

$$\|w\|_{H^1(B)} \leqslant C\omega\|\varphi\|_{L^2(B)}. \tag{2.12}$$

Using the operator A, we can see that problem (2.9) is equivalent to find $u \in L^2(B)$ such that

$$(I - \omega^2 A)u = w. \tag{2.13}$$

When the frequency ω is small enough, the operator $I - \omega^2 A$ has a uniformly bounded inverse. We then have the estimate

$$\|u\|_{L^2(B)} \leqslant C\|w\|_{L^2(B)}, \tag{2.14}$$

where the constant C is independent of ω. Rearranging (2.13), we have $u = w - \omega^2 Au$, so $u \in H^1(B)$ and, by the estimate (2.11) for the operator A, we have

$$\|u\|_{H^1(B)} \leqslant \|w\|_{H^1(B)} + C\omega^2\|u\|_{L^2(B)}.$$

The proof is complete by combining the above estimate and (2.12). □

It is evident that the determination of the scatterer function q from some boundary measurement of the wave field u from equation (2.3) is a nonlinear problem. We consider an approximate problem and derive an error estimate between the solution of the approximate problem and the solution of the original scattering problem. The error estimate is crucial for the derivation of initial guesses. Dropping the nonlinear term in equation (2.3) yields

$$\Delta u_{\mathrm{B}} + \omega^2 u_{\mathrm{B}} = \mathrm{i}\omega\varphi, \tag{2.15}$$

where u_{B} is required to satisfy the Sommerfeld radiation condition.

The approximate problem has an equivalent weak formulation: find $u_{\mathrm{B}} \in H^1(B_R)$ such that

$$a_{\mathrm{B}}(u_{\mathrm{B}}, v) = b(v) \qquad \text{for all} \quad v \in H^1(B_R), \tag{2.16}$$

where the bilinear form $a_{\mathrm{B}} : H^1(B_R) \times H^1(B_R) \to \mathbb{C}$

$$a_{\mathrm{B}}(u, v) = (\nabla u, \nabla v) - \omega^2\,(u, v) - \langle Tu, v\rangle,$$

and the linear functional are given in equation (2.8).

Theorem 2.2. *If the frequency ω is sufficiently small, the variational problem (2.16) admits a unique weak solution u_B in $H^1(B_R)$. It holds*

$$\|u - u_{\mathrm{B}}\|_{H^1(B_R)} \leqslant C\omega^3\|q\|_{L^\infty(B_R)}\|\varphi\|_{L^2(B_R)}, \tag{2.17}$$

where u is the solution of the variational problem (2.9) and C is a frequency-independent positive number.

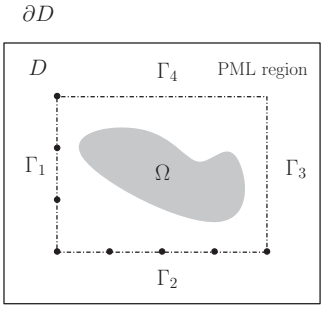

Figure 2. Geometry of the scattering problem with the PML layer.

Proof. Let $w = u - u_{\mathrm{B}}$. Subtracting equation (2.15) from equation (2.3) yields

$$\begin{aligned} &\Delta w + \omega^2 w = -\omega^2 q u \qquad \text{in} \quad B, \\ &\partial_{\mathbf{n}} w = T w \qquad \text{on} \quad \partial B. \end{aligned}$$

It follows from theorem 2.1 that the above problem has a unique weak solution in $H^1(B_R)$ and the solution has the energy estimate

$$\|w\|_{H^1(B_R)} \leqslant C\omega^2 \|q\|_{L^\infty(B)} \|u\|_{L^2(B_R)},$$

where the positive number C is independent of the frequency.

A direct application of the energy estimate for u in equation (2.10) gives

$$\|w\|_{H^1(B)} \leqslant C\omega^3 \|q\|_{L^\infty(B)} \|\varphi\|_{L^2(B)},$$

which completes the proof. □

The error estimate (2.17) implies that u_{B} is a good approximation to u for a small frequency ω.

2.3. PML formulation

The converted deterministic problem is imposed in the open domain. In practice, the open domain needs to be truncated into a bounded domain. Therefore, a suitable boundary condition has to be imposed on the boundary of the bounded domain so that no artificial wave reflection occurs. In the previous section, the DtN operator does give a transparent boundary condition. However, this non-reflecting boundary condition is nonlocal and involves the issue of truncation of an infinity series. Computationally, we employ a convenient uniaxial PML technique to truncate the open domain into a bounded rectangular domain, as seen in figure 2.

Next we introduce the absorbing PML and formulate the scattering problem in a bounded domain. Let D be the rectangle which contains Ω and let d_1 and d_2 be the thickness of the PML layers along x and y, respectively. Denote by ∂D the boundary of the domain D. Let $s_1(x) = 1 + \mathrm{i}\sigma_1(x)$ and $s_2(y) = 1 + \mathrm{i}\sigma_2(y)$ be the model medium property, where σ_j are the positive continuous even functions and satisfy $\sigma_j(x) = 0$ in Ω.

Following the general idea in designing PML absorbing layers, we may deduce the truncated PML problem: find the PML solution, still denoted as u, to the following system:

$$\begin{aligned} &\nabla \cdot (s \nabla u) + s_1 s_2 \omega^2 (1+q) u = \mathrm{i}\omega\varphi \qquad \text{in} \quad D, \\ &u = 0 \qquad \text{on} \quad \partial D, \end{aligned} \tag{2.18}$$

where $s = \mathrm{diag}(s_2(y)/s_1(x), s_1(x)/s_2(y))$ is a diagonal matrix. The variational problem can be formulated to find $u \in H_0^1(D) = \{u \in H^1(D) : u = 0 \text{ on } \partial D\}$ such that

$$a_{\mathrm{PML}}(u, v) = b(v) \qquad \text{for all} \quad v \in H_0^1(D), \tag{2.19}$$

where the bilinear form $a_{\mathrm{PML}} : H_0^1(D) \times H_0^1(D) \to \mathbb{C}$

$$a_{\mathrm{PML}}(u, v) = (s\nabla u, \nabla v) - \omega^2(s_1 s_2(1+q)u, v), \tag{2.20}$$

and the linear functional b is defined in equation (2.8).

Denote the physical domain Ω by the rectangle $[x_1, x_2] \times [y_1, y_2]$. The computational domain is then $D = [x_1 - d_1, x_2 + d_1] \times [y_1 - d_2, y_2 + d_2]$. The model medium property is usually taken as a power function:

$$\sigma_1(x) = \begin{cases} \sigma_0 \left(\dfrac{x - x_2}{d_1} \right)^p & \text{for } x_2 < x < x_2 + d_1 \\ 0 & \text{for } x_1 \leqslant x \leqslant x_2 \\ \sigma_0 \left(\dfrac{x_1 - x}{d_1} \right)^p & \text{for } x_1 - d_1 < x < x_1, \end{cases}$$

and

$$\sigma_2(y) = \begin{cases} \sigma_0 \left(\dfrac{y - y_2}{d_2} \right)^p & \text{for } y_2 < y < y_2 + d_2 \\ 0 & \text{for } y_1 \leqslant y \leqslant y_2 \\ \sigma_0 \left(\dfrac{y_1 - y}{d_2} \right)^p & \text{for } y_1 - d_2 < y < y_1, \end{cases}$$

where the constant $\sigma_0 > 1$ and the integer $p \geqslant 2$.

The well-posedness of the PML problem (2.19) and the convergence of its solution to the solution of the original scattering problem (2.1) are studied in [22]. The error estimate particularly implies that the PML solution converges exponentially to the original scattering problem when either the PML medium parameter σ_0 or the thicknesses d_1 and d_2 of the layer are increased. Therefore, we may choose σ_0 and d_1, d_2 such that the PML model problem error is negligible compared with the finite-element discretization errors.

3. Inverse scattering problem

In this section, the RLM for the inverse medium scattering problem is presented. The algorithm, obtained by a continuation method on the frequency, requires multi-frequency scattering data. At each frequency, the algorithm determines a forward model which produces the prescribed scattering data. At a low frequency, the scattered field is weak. Consequently, the nonlinear equation becomes essentially linear, known as the Born approximation. The algorithm first solves this nearly linear equation at the lowest frequency to obtain low-frequency modes of the true scatterer. The approximation is then used to linearize the nonlinear equation at the next higher frequency to produce a better approximation which contains more modes of the true scatterer. This process is continued until a sufficiently high frequency where the dominant modes of the scatterer are essentially recovered.

3.1. Born approximation

To initialize the recursive linearization method, a starting point or an initial guess is needed which is derived from the Born approximation. The starting point will be derived from different linear integrals, depending on the availability of the data.

Rewrite equation (2.3) as

$$\Delta u + \omega^2 u = \mathrm{i}\omega\varphi - \omega^2 q u.$$

According to theorem 2.2, we may replace u on the right-hand side by u_{B} for a sufficiently small frequency to get an approximate equation

$$\Delta u + \omega^2 u = \mathrm{i}\omega\varphi - \omega^2 q u_{\mathrm{B}}, \tag{3.1}$$

which is called the Born approximation.

If the wave field u is available on the whole boundary of B_R, the plane waves turn out to be useful to obtain an initial guess. Consider an auxiliary function $u^{\mathrm{inc}}(\mathbf{x}) = \mathrm{e}^{\mathrm{i}\omega\mathbf{x}\cdot\mathbf{d}}$, $\mathbf{d} = (\cos\tau, \sin\tau)$, $\tau \in [0, 2\pi]$. This auxiliary function represents propagating plane waves and satisfies the Helmholtz equation

$$\Delta u^{\mathrm{inc}} + \omega^2 u^{\mathrm{inc}} = 0 \qquad \text{in} \quad \mathbb{R}^2.$$

Multiplying equation (3.1) by u^{inc} and integrating over B_R on both sides, we have

$$\int_{B_R} \Delta u u^{\mathrm{inc}} + \omega^2 \int_{B_R} u u^{\mathrm{inc}} = \mathrm{i}\omega \int_{B_R} \varphi u^{\mathrm{inc}} - \omega^2 \int_{B_R} q u_{\mathrm{B}} u^{\mathrm{inc}}.$$

Integration by parts gives

$$\int_{\partial B_R} (u^{\mathrm{inc}} \partial_{\mathbf{n}} u - u \partial_{\mathbf{n}} u^{\mathrm{inc}}) = \mathrm{i}\omega \int_{B_R} \varphi u^{\mathrm{inc}} - \omega^2 \int_{B_R} q u_{\mathrm{B}} u^{\mathrm{inc}}.$$

Using the DtN operator (2.5), we obtain a linear integral equation for the scatterer q:

$$\int_{B_R} q u_{\mathrm{B}}\, u^{\mathrm{inc}} = \frac{\mathrm{i}}{\omega} \int_{B_R} \varphi\, u^{\mathrm{inc}} + \frac{1}{\omega^2} \int_{\partial B_R} (u \partial_{\mathbf{n}} u^{\mathrm{inc}} - u^{\mathrm{inc}} T u), \tag{3.2}$$

where the right-hand side of equation (3.2) can be treated as the input data since the wave field u is known all around ∂B_R.

Alternatively, the following approach can be employed even if the wave field u is only available in the limited aperture case. Consider the fundamental solution of the Helmhotlz equation in two-dimensional space:

$$G(\mathbf{x}, \mathbf{y}) = \frac{\mathrm{i}}{4} H_0^{(1)}(\omega|\mathbf{x} - \mathbf{y}|).$$

Using this fundamental solution, we obtain from equation (3.1) that the wave field satisfies the Lippmann–Schwinger integral equation

$$u(\mathbf{x}) = \omega^2 \int_B G(\mathbf{x}, \mathbf{y}) u_{\mathrm{B}}(\mathbf{y}) q(\mathbf{y})\, \mathrm{d}\mathbf{y} - \mathrm{i}\omega \int_B G(\mathbf{x}, \mathbf{y}) \varphi(\mathbf{y})\, \mathrm{d}\mathbf{y},$$

which gives a linear integral equation for the scatterer q:

$$\int_{B_R} G(\mathbf{x}, \mathbf{y}) u_{\mathrm{B}}(\mathbf{y}) q(\mathbf{y})\, \mathrm{d}\mathbf{y} = \frac{1}{\omega^2} u(\mathbf{x}) + \frac{\mathrm{i}}{\omega} \int_{B_R} G(\mathbf{x}, \mathbf{y}) \varphi(\mathbf{y})\, \mathrm{d}\mathbf{y}. \tag{3.3}$$

In practice, the linear integral equation (3.2) or (3.3) is implemented by using the method of least squares with the Tikhonov regularization, which leads to a starting point for our recursive linearization method.

3.2. Recursive linearization

We now describe the procedure that recursively determines better approximations q_ω at $\omega = \omega_k$ for $k = 1, 2, \ldots$ with the increasing frequencies. The procedure will be given for the Helmholtz equation with PML problem, since this is what we numerically implement. Suppose now that an approximation of the scatterer, $q_{\tilde{\omega}}$, has been recovered at some wavenumber $\tilde{\omega}$, and that the wavenumber ω is slightly larger that $\tilde{\omega}$. We wish to determine q_ω, or equivalently, to determine the perturbation

$$\delta q = q_\omega - q_{\tilde{\omega}}. \tag{3.4}$$

For the reconstructed scatterer $q_{\tilde{\omega}}$, we solve at the frequency ω the direct scattering problem

$$\begin{aligned} &\nabla \cdot (s\nabla u) + s_1 s_2 \omega^2 (1 + q_{\tilde{\omega}})u = \mathrm{i}\omega\varphi \qquad \text{in} \quad D, \\ &u = 0 \qquad \text{on} \quad \partial D. \end{aligned} \tag{3.5}$$

For the scatterer q_ω, we have

$$\begin{aligned} &\nabla \cdot (s\nabla(u + \delta u)) + s_1 s_2 \omega^2 (1 + q_\omega)(u + \delta u) = \mathrm{i}\omega\varphi \qquad \text{in} \quad D, \\ &u + \delta u = 0 \qquad \text{on} \quad \partial D. \end{aligned} \tag{3.6}$$

Subtracting (3.5) from (3.6) and omitting the second-order smallness in δq and in δu, we obtain

$$\begin{aligned} &\nabla \cdot (s\nabla \delta u) + s_1 s_2 \omega^2 (1 + q_{\tilde{\omega}})\delta u = -\delta q s_1 s_2 \omega^2 u \qquad \text{in} \quad D, \\ &\delta u = 0 \qquad \text{on} \quad \partial D. \end{aligned} \tag{3.7}$$

Given a solution u of (3.5), we define the measurements

$$Mu(\mathbf{x}) = [u(\mathbf{x}_1), \ldots, u(\mathbf{x}_n)]^\top, \tag{3.8}$$

where $\mathbf{x}_i$, $i = 1, \ldots, n$, are the points where the wave field u is measured. The measurement operator M is well defined and maps the electric field to a vector of complex numbers in $\mathbb{C}^n$, which consists of point measurements of the scattered field at $\mathbf{x}_i$, $i = 1, \ldots, n$.

For the scatterer q_ω and the source field φ, we define the forward scattering operator

$$S(q_\omega, \varphi) = Mu. \tag{3.9}$$

It is easily seen that the forward scattering operator $S(q_\omega, \varphi)$ is linear with respect to φ but nonlinear with respect to q_ω. For simplicity, we denote $S(q_\omega, \varphi)$ by $S(q_\omega)$. Let $S'(q_{\tilde{\omega}})$ be the Fréchet derivative of $S(q_\omega)$ and denote the residual operator

$$R(q_{\tilde{\omega}}) = M(\delta u). \tag{3.10}$$

It follows from the linearization of the nonlinear equation (3.9) that

$$S'(q_{\tilde{\omega}})\delta q = R(q_{\tilde{\omega}}). \tag{3.11}$$

Applying the Landweber–Kaczmarz iteration [34] to the linearized equation (3.11) yields

$$\delta q = \beta \,\mathrm{Re}\, S'(q_{\tilde{\omega}})^* R(q_{\tilde{\omega}}), \tag{3.12}$$

where β is a positive relaxation parameter and $S'(q_{\tilde{\omega}})^*$ is the adjoint operator of $S'(q_{\tilde{\omega}})$.

Remark 3.1. The Landweber–Kaczmarz iteration process is taken with respect to the orthonormal basis functions ϕ_i and ψ_j for $i, j = 1, \ldots, m$. The Landweber–Kaczmarz method usually displays better convergence property than the simple Landweber iteration. The relation between the Landweber iteration and Landweber–Kaczmarz is of the same type as between the Jacobi and Gauss–Seidel iteration for linear systems.

In order to compute the correction δq, we need an efficient way to compute $S'(q_{\tilde{\omega}})^* R(q_{\tilde{\omega}})$. Let $R(q_{\tilde{\omega}}) = [\zeta_1, \ldots, \zeta_n]^\top \in \mathbb{C}^n$. Consider the adjoint problem

$$\begin{aligned} &\nabla \cdot (\bar{s}\nabla v) + \bar{s}_1\bar{s}_2\omega^2(1+q_{\tilde{\omega}})v = -\omega^2 \sum_{i=1}^{n} \delta(\mathbf{x}-\mathbf{x}_n)\zeta_i \qquad \text{in} \quad D, \\ &v = 0 \qquad \text{on} \quad \partial D. \end{aligned} \tag{3.13}$$

Multiplying (3.7) with the complex conjugate of v and integrating over D on both sides, we obtain

$$\int_D \nabla \cdot (s\nabla \delta u)\bar{v} + \omega^2 \int_\Omega s_1 s_2 (1+q_{\tilde{\omega}})\delta u \bar{v} = -\omega^2 \int_\Omega \delta q\, s_1 s_2 u \bar{v}.$$

Using Green's formula and the homogeneous Dirichlet boundary conditions in equations (3.7) and (3.13) yields

$$\int_\Omega \delta u[\nabla \cdot (s\nabla \bar{v}) + s_1 s_2 \omega^2 (1+q_{\tilde{\omega}})\bar{v}] = -\omega^2 \int_\Omega \delta q\, s_1 s_2 u \bar{v}.$$

Taking the complex conjugate of equation (3.13) and plugging into the above equation gives

$$-\omega^2 \sum_{i=1}^{n} \int_\Omega \delta u \delta(\mathbf{x}-\mathbf{x}_i)\bar{\zeta}_i = -\omega^2 \int_\Omega \delta q\, s_1 s_2 u \bar{v},$$

which implies

$$\sum_{i=1}^{n} \delta u(\mathbf{x}_i)\bar{\zeta}_i = \int_\Omega \delta q\, s_1 s_2 u \bar{v}. \tag{3.14}$$

Noting (3.10), (3.11) and the adjoint operator $S'(q_{\tilde{\omega}})^*$, the left-hand side of (3.14) may be deduced:

$$\sum_{i=1}^{n} \delta u(\mathbf{x}_i)\bar{\zeta}_i = \langle M(\delta u), R(q_{\tilde{\omega}})\rangle_{\mathbb{C}^n} = \langle S'(q_{\tilde{\omega}})\delta q, R(q_{\tilde{\omega}})\rangle_{\mathbb{C}^n} \tag{3.15}$$

$$= \langle \delta q, S'(q_{\tilde{\omega}})^* R(q_{\tilde{\omega}})\rangle_{L^2(\Omega)} = \int_\Omega \delta q \overline{S'(q_{\tilde{\omega}})^* R(q_{\tilde{\omega}})}, \tag{3.15}$$

where $\langle\cdot,\cdot\rangle_{\mathbb{C}^n}$ and $\langle\cdot,\cdot\rangle_{L^2(\Omega)}$ are the standard inner products defined in the complex vector space $\mathbb{C}^n$ and the square integrable functional space $L^2(\Omega)$.

Combining (3.14) and (3.15) yields

$$\int_\Omega \delta q\, s_1 s_2 u \bar{v} = \int_\Omega \delta q \overline{S'(q_{\tilde{\omega}})^* R(q_{\tilde{\omega}})},$$

which holds for any δq. It follows that

$$S'(q_{\tilde{\omega}})^* R(q_{\tilde{\omega}}) = \bar{s}_1\bar{s}_2\overline{u}v. \tag{3.16}$$

Using the above result, equation (3.12) can be written as

$$\delta q = \beta\, \mathrm{Re}\, \bar{s}_1\bar{s}_2\overline{u}v. \tag{3.17}$$

Thus, for each pair of sources ϕ_i and ψ_j, we solve one direct problem (3.5) and one adjoint problem (3.13). Once δq is determined, q_ω is updated by $q_{\tilde{\omega}} + \delta q$. After completing the sweep for all sources $\phi_i, \psi_j, i, j = 1, \ldots, m$, we get the reconstructed scatterer function q_ω at the frequency ω.

If the scattering data contain noise, the semi-convergence of the gradient-based algorithm can be observed: the algorithm firstly converges to certain level and then starts to diverge. This phenomenon illustrates the ill-posedness of the inverse scattering problem. Therefore,

some regularization technique is required to stabilize the iteration. For instance, if the noise level is known, the discrepancy principle may be used as a stopping rule for detecting the transient from convergence to divergence. To stabilize the iterative we will examine the RLM from the optimization point of view in the next section, which also provides an explicit way to add the regularization term.

3.3. Adjoint state approach

Consider the inverse medium scattering problem as the following minimization process:

$$\min[F(q) + \alpha N(q)],$$

where F is the objective functional, α is the regularization parameter and the regularization functional N can be taken as the L_2 regularization

$$N(q) = \frac{1}{2}\int_D |\nabla q|^2$$

for a smooth scatterer function q and L_1 regularization

$$N(q) = \frac{1}{2}\int_D \sqrt{|\nabla q|^2 + \gamma}$$

for the nonsmooth scatterer function q, where γ is a small smoothing parameter avoiding zero denominator in the following evaluations.

To minimize the cost functional by a gradient method, it is required to compute the Fréchet derivatives of the objective functional and the regularization functionals. Noting the compact support of the scatterer q and using integration by parts, we may obtain the Fréchet derivatives of the regularization functional

$$N'(q) = \Delta q \tag{3.18}$$

for the smooth scatterer q and

$$N'(q) = \nabla \cdot \left(\frac{\nabla q}{\sqrt{|\nabla q|^2 + \gamma}} \right) \tag{3.19}$$

for the nonsmooth scatterer q.

Next we consider the objective functional F, which can be formulated as

$$F(q) = \frac{1}{2}\sum_{i=1}^{n} |u(q)(\mathbf{x}_i) - u(\mathbf{x}_i)|^2, \tag{3.20}$$

where $u(q)$ is the solution of the PML problem (2.18) with the scatterer q and $u(\mathbf{x}_i)$, $i = 1, \ldots, n$, are data points. Let

$$u(q)(\mathbf{x}_i) - u(\mathbf{x}_i) = [\zeta_1, \ldots, \zeta_n]^\top \in \mathbb{C}^n.$$

A simple calculation yields the derivative of the cost functional at q:

$$F'(q)\delta q = \mathrm{Re}\sum_{i=1}^{n} \langle u'(q)\delta q\rangle(\mathbf{x}_i)\,\bar{\zeta}_i, \tag{3.21}$$

where $\langle u'(q)\delta q\rangle$ is the Fréchet derivative of u at q, satisfying

$$\begin{aligned} &\nabla \cdot (s\nabla\langle u'(q)\delta q\rangle) + s_1 s_2 \omega^2 (1+q)\langle u'(q)\delta q\rangle = -\omega^2 \delta q s_1 s_2 u \qquad \text{in} \quad D, \\ &\langle u'(q)\delta q\rangle = 0 \qquad \text{on} \quad \partial D. \end{aligned} \tag{3.22}$$

To compute the Fréchet derivative, we introduce the adjoint state system:

$$\begin{aligned} &\nabla \cdot (\bar{s}\nabla v) + \bar{s}_1\bar{s}_2\omega^2(1+q)v = -\omega^2 \sum_{i=1}^{n} \delta(\mathbf{x}-\mathbf{x}_i)\zeta_i \qquad \text{in} \quad D, \\ &v = 0 \qquad \text{on} \quad \partial D. \end{aligned} \tag{3.23}$$

Multiplying equation (3.22) with the complex conjugate of v on both sides and integrating over D yields

$$\int_D \nabla \cdot (s\nabla\langle u'(q)\delta q\rangle)\bar{v} + \omega^2 \int_D s_1 s_2(1+q)\langle u'(q)\delta q\rangle \bar{v} = -\omega^2 \int_D \delta q\, s_1 s_2 u\bar{v}.$$

Noting the Dirichlet boundary conditions in (3.22) and (3.23), we deduce from the integration by parts that

$$\int_D \langle u'(q)\delta q\rangle[\nabla \cdot (s\nabla\bar{v}) + s_1 s_2\omega^2(1+q)\bar{v}] = -\omega^2 \int_D \delta q s_1 s_2 u\bar{v}.$$

Taking complex conjugate of equation (3.23) and plugging into the above equation gives

$$-\omega^2 \sum_{i=1}^{n} \int_D \langle u'(q)\delta q\rangle \delta(\mathbf{x}-\mathbf{x}_i)\bar{\zeta}_i = -\omega^2 \int_D \delta q\, s_1 s_2 u\bar{v},$$

which implies

$$\sum_{i=1}^{n} \langle u'(q)\delta q\rangle(\mathbf{x}_i)\,\bar{\zeta}_i = \int_D \delta q\, s_1 s_2 u\bar{v}. \tag{3.24}$$

Combining equations (3.21) and (3.24), we obtain

$$F'(q)\delta q = \operatorname{Re} \int_D \delta q\, s_1 s_2 u\bar{v},$$

which gives the Fréchet derivative of the cost functional

$$F'(q) = \operatorname{Re}\, \bar{s}_1\bar{s}_2\bar{u}v. \tag{3.25}$$

Comparing equations (3.17) and (3.25), we derive the same Fréchet derivative from different points of view: one is described via operator equations and another is based on the optimization approach. The optimization process gives a natural way to regularize the ill-posed problem and make the method of the recursive linearization stable.

3.4. Reconstruction implementations

First we comment on the scattering data and the direct solver. The scattering data were obtained by the numerical solution of the direct scattering problem, which was implemented by using the finite-element method with the uniaxial PML technique. The sparse large-scale linear system can be most efficiently solved if the zero elements of the coefficient matrix are not stored. We use the commonly used compressed row storage format which makes no assumptions about the sparsity structure of the matrix, and does not store any unnecessary elements. In fact, from the variational formula of our direct problem, the coefficient matrix is complex symmetric. Hence, only the lower triangular portion of the matrix needs be stored. Regarding the linear solver, the quasi-minimal residual algorithm with diagonal preconditioning was employed to solve the sparse, symmetric and complex system of the equations.

Next, we present an outline of the algorithm in table 1. After inputting the user-specified parameters, such as the minimum frequency $\omega_{\min}$, the maximum frequency $\omega_{\max}$, the PML model medium property σ_0, power p, thicknesses d_1 and d_2, the relaxation parameter α, the

Table 1. Outline of the recursive linearization algorithm.

```
program main
input user-specified parameters: ω_min, ω_max, p, m, σ_0, d_1, d_2, α, β, γ
generate an initial guess from the Born approximation at ω_max
for ω = ω_min : ω_max
    for i = 1 : m
    for j = 1 : m
        solve one direct problem
        solve one adjoint problem
        compute the Fréchet derivative of the regularization functional
        update the scatterer function
    end for
    end for
end for
end main
```

regularization parameter β and the smoothing parameter γ, the code generates an initial guess from the Born approximation at the lowest frequency $\omega_{\min}$. Then the code loops over the frequency from the lowest to the highest. At each frequency, two inner loops are done for the orthonormal basis functions. At each iteration, we directly compute the Fréchet derivative of the regularization functional, solve one direct and one adjoint problem to obtain the Fréchet derivative of the objective functional and update the scatterer function. The overall computational complexity is the number of direct solvers, which is the number of frequencies times twice of the number of the orthonormal basis functions, besides a small fraction of the CPU time used for solving the linear integral equation to generate the initial guess.

4. Numerical results

The code was written in Fortran90 using double precision arithmetic and was compiled using the ifort compiler. The computations were run on an Intel Pentium 4 processor (3.2 GHz, 1536MB memory). In this section, we present three numerical examples to illustrate the performance of the method.

Example 1. Let

$$q(x, y) = 5x^2 y\, \mathrm{e}^{-(x^2+y^2)},$$

reconstruct a scatterer defined by

$$q_1(x, y) = q(3x, 3y)$$

inside the rectangular physical domain $\Omega = [-1, 1] \times [-1, 1]$, see figure 3 for surface and contour plots of the scatterer function in the domain Ω. The physical domain Ω was partitioned into 7200 equal triangular elements. The computational domain D was obtained from the physical domain by adding 20 grid points absorbing PML layers at each direction of x and y, which leads to 20 000 equal triangular elements. Ten equally spaced frequencies were used in the reconstruction, starting from the lowest frequency $\omega_{\min} = 0.5\pi$ (corresponding to the wavelength $\lambda = 4.0$) and ending at the highest frequency $\omega_{\max} = 5.0\pi$ (corresponding to the wavelength $\lambda = 0.4$). Denote by $\Delta\omega = (\omega_{\max} - \omega_{\min})/9$ the stepsize of the frequency; then the ten equally space frequencies are $\omega_j = \omega_{\min} + j\Delta\omega$, $j = 0, \ldots, 9$. The number

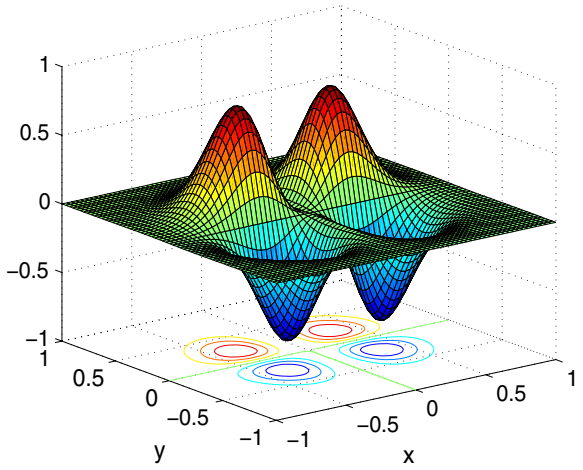

Figure 3. Surface and contour views of the exact scatterer q_1 for example 1.

Table 2. Relative $L^2(\Omega)$ error of reconstruction at ten frequencies for example 1.

ω	ω_0	ω_1	ω_2	ω_3	ω_4
e_2	9.84×10^{-1}	8.06×10^{-1}	4.62×10^{-1}	1.99×10^{-1}	7.30×10^{-2}
ω	ω_5	ω_6	ω_7	ω_8	ω_9
e_2	3.46×10^{-2}	2.54×10^{-2}	2.17×10^{-2}	2.01×10^{-2}	1.92×10^{-2}

Table 3. Relative $L^2(\Omega)$ error of reconstruction at ten set of basis functions for example 1.

m	1	2	3	4	5
e_2	8.29×10^{-1}	4.23×10^{-1}	1.73×10^{-1}	3.85×10^{-2}	2.51×10^{-2}
m	6	7	8	9	10
e_2	2.15×10^{-2}	1.99×10^{-2}	1.92×10^{-2}	1.89×10^{-2}	1.87×10^{-2}

of orthonormal basis functions were taken as $m = 8$, which accounts for 64 Landweber–Kaczmarz iterations at each frequency. The relaxation parameter β is 0.01. The L_2 regularization functional was used for this smooth scatterer function and the regularization parameter α is 10^{-4}. The inversion method reconstructed it accurately. The reconstructed function will not be plotted against the exact scatterer since the error is so small that it is invisible in the plot. The procedure costs 1029 s CPU time, see table 2 for the relative $L^2(\Omega)$ error of the reconstruction at ten frequencies. It clearly shows a convergence of the method as the frequency increases. Table 3 investigates the reconstruction at ten set of basis functions. It displays a rapid decay of the reconstruction error for the first few set of basis functions and then tends to maintain at a certain error level with slow decay. It suggests that a few set of basis functions are sufficient to reach certain accuracy, which reduces the computational complexity.

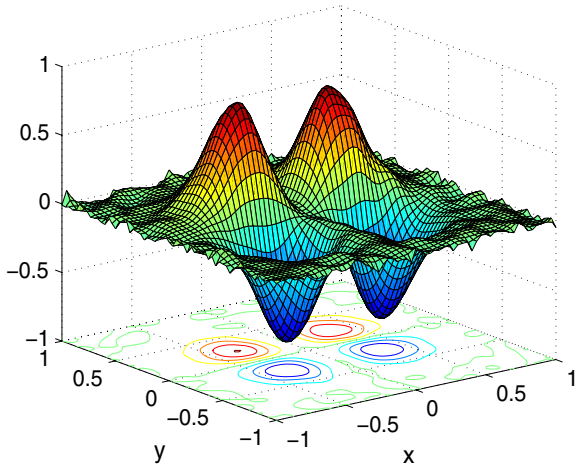

Figure 4. Surface and contour views of reconstructed scatterer q_1 for example 1.

Table 4. Relative $L^2(\Omega)$ error of reconstruction with noisy data for example 1.

σ	1%	5%	10%	15%	20%
e_2	1.98×10^{-2}	2.88×10^{-2}	4.67×10^{-2}	6.63×10^{-2}	8.66×10^{-2}

To test the stability of the method, we reconstruct the scatterer q_1 with noisy data. Some relative random noise is added to the date, i.e. the scattering data takes

$$u := (1 + \sigma \text{ rand})u.$$

Here, rand gives uniformly distributed random numbers in $[-1, 1]$ and σ is a noise level parameter. Five tests were made here corresponding to the noise level added into the scattering data to $\sigma = 1\%, 5\%, 10\%, 15\%, 20\%$. The resulting errors in the inversion are listed in table 4. Figure 4 shows the surface and contour plots of the reconstruction with the scattering data corresponding to the noisy level $\sigma = 20\%$. It actually reconstructed the scatterer with a 8.66% relative error. The stability tests show that the method is not sensitive to the data noise.

Example 2. Reconstruct a scatterer defined in the rectangular domain Ω by

$$q_2(x, y) = \begin{cases} q(4x, 4y) & \text{for} \quad \rho < 0.7 \\ -0.5 & \text{for} \quad 0.7 \leqslant \rho \leqslant 0.9. \\ 0.0 & \text{for} \quad \rho > 0.9 \end{cases}$$

See figure 5 for surface and contour plots of the function. This scatterer is difficult to reconstruct since the function is discontinuous across two circles $\rho = 0.7$ and $\rho = 0.9$. The value of the function changes sharply to -0.5 in the narrow annulus. A finer mesh and a higher maximum frequency were used to capture more detailed information for this example. The physical domain Ω was partitioned into 12 800 equal triangular elements. The computational domain D was obtained from the physical domain by adding 20 grid points absorbing PML layers at each direction of x and y, which leads to 28 800 equal triangular elements. Twelve equally spaced frequencies were used in the reconstruction, starting from the lowest frequency $\omega_{\min} = 0.5\pi$ and ending at the highest frequency $\omega_{\max} = 8.0\pi$ (corresponding to the wavelength $\lambda = 0.25$).

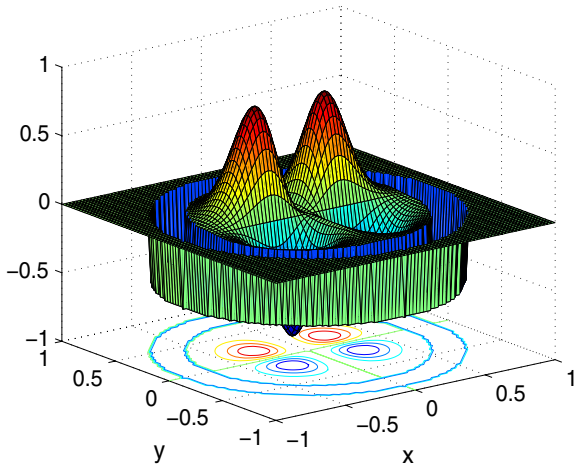

Figure 5. Surface and contour views of exact scatterer q_2 for example 2.

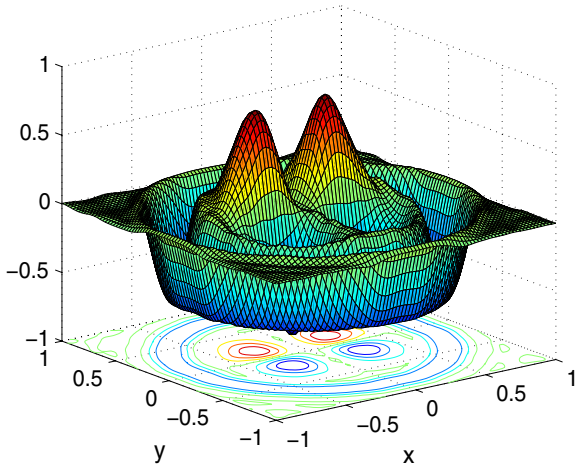

Figure 6. Surface and contour views of reconstructed scatterer q_2 for example 2.

Denote by $\Delta\omega = (\omega_{\max} - \omega_{\min})/11$ the stepsize of the frequency; then the 12 equally space frequencies are $\omega_j = \omega_{\min} + j\Delta\omega$, $j = 0, \ldots, 11$. The number of orthonormal basis functions were taken as $m = n = 8$, which accounts for 64 Landweber–Kaczmarz iterations at each frequency. The L_1 regularization functional was used for this nonsmooth scatterer function and the smoothing parameter γ is 10^{-6}. Since the mesh is finer, the relaxation parameter β is taken as a smaller number 0.001 to maintain the stability of the method. The procedure costs 3107 s CPU time. The relative $L^2(\Omega)$ error of the reconstruction at the 12 frequencies is listed in table 5. Figure 6 shows the surface and contour plots of the reconstructed scatterer with eight sets of basis functions, whereas figure 7 shows a cross-section reconstruction of the scatterer at $x = -0.3$. An examination of the plots shows that the error of the reconstructions occurs largely around the discontinuities, while the smooth part is recovered more accurately.

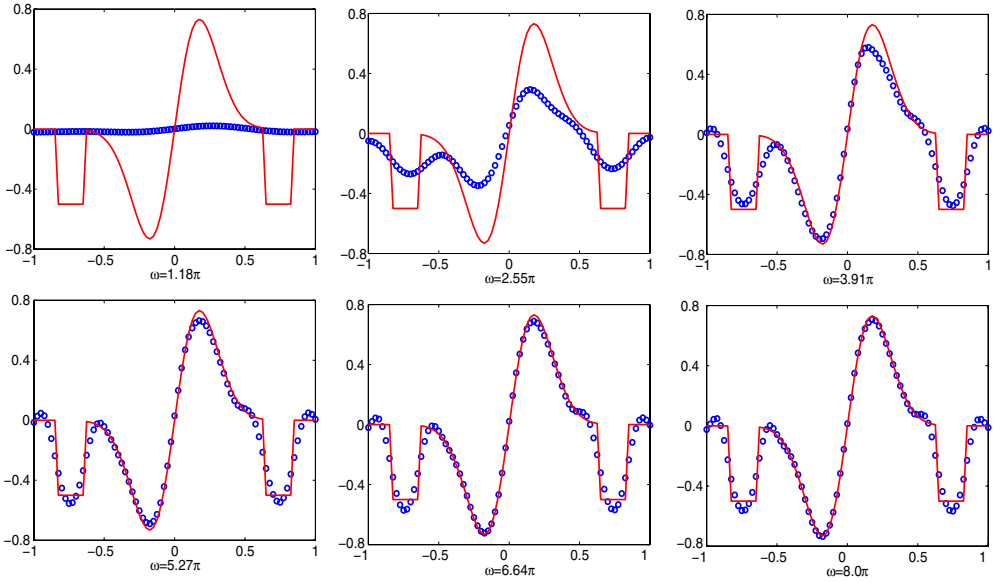

Figure 7. Cross section of reconstructed again exact scatterer q_2 at six frequencies for example 2.

Table 5. Relative $L^2(\Omega)$ error of reconstruction at 12 frequencies for example 2.

ω	ω_0	ω_1	ω_2	ω_3	ω_4	ω_5
e_2	9.97×10^{-1}	9.67×10^{-1}	8.15×10^{-1}	6.13×10^{-1}	4.19×10^{-1}	3.18×10^{-1}
ω	ω_6	ω_7	ω_8	ω_9	ω_{10}	ω_{11}
e_2	2.77×10^{-1}	2.62×10^{-1}	2.55×10^{-1}	2.51×10^{-2}	2.48×10^{-1}	2.44×10^{-1}

Table 6. Relative $L^2(\Omega)$ error of reconstruction at ten frequencies for example 3.

ω	ω_0	ω_1	ω_2	ω_3	ω_4
e_2	9.97×10^{-1}	9.49×10^{-1}	7.89×10^{-1}	5.63×10^{-1}	3.73×10^{-1}
ω	ω_5	ω_6	ω_7	ω_8	ω_9
e_2	2.65×10^{-1}	2.12×10^{-1}	1.82×10^{-1}	1.62×10^{-1}	1.43×10^{-1}

Example 3. Reconstruct the scatterer q_1 with limited aperture data. The wavefield u is only available on the line segment of Γ_3, i.e. one side boundary of the physical domain Ω, as seen in figure 1. This is a quite severe test to a method since the inverse problem becomes even more ill-posed without full aperture data. We used the same parameters as those in example 1, i.e. 20 000 equal triangular elements, ten equally spaced frequencies varying from $\omega_{\min} = 0.5\pi$ to $\omega_{\max} = 5.0\pi$, the number of orthonormal basis functions $m = 8$, the relaxation parameter $\beta = 0.01$. Table 6 shows the relative $L^2(\Omega)$ error of the reconstruction at ten frequencies, see figure 8 for the surface and contour plots of the reconstructed scatterer.

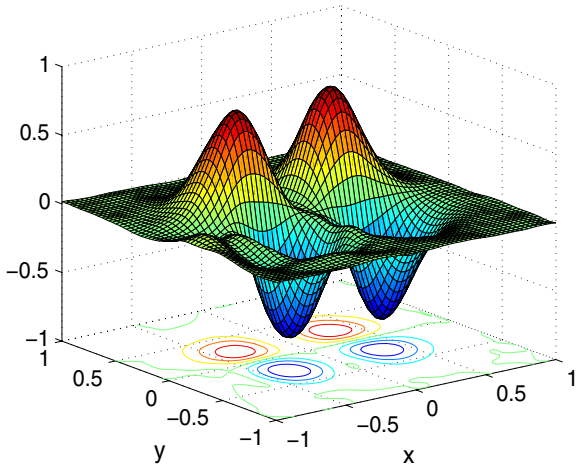

Figure 8. Surface and contour views of reconstructed scatterer q_1 for example 3.

5. Conclusion

We presented a recursive linearization method for solving the inverse medium scattering problem with a stochastic source. Based on WCE theory, we converted the two-dimensional Helmholtz equation with a stochastic source into a set of equations with deterministic sources. For the deterministic model problem, we analyzed the direct scattering problem using DtN map and provided some energy estimates for the wave fields. Computationally, we employed a finite-element method with an uniaxial PML technique to truncate the open domain into a bounded cell. The recursive linearization method requires multi-frequency scattering data. It starts with an initial guess from the Born approximation and each update is obtained via a continuation procedure on the frequency by solving one direct and one adjoint problem of the Helmholtz equation. We considered two types of example, smooth and non-smooth scatterer functions, and two types of scattering data, full and limited aperture. The reconstruction error and stability tests were reported at different frequencies and different sets of basis functions. The method of combining WCE with recursive linearization is robust and efficient for solving the inverse medium problem with a stochastic source.

We point out some future directions along the line of this work. An interesting and challenging problem is to solve the inverse medium problem with a stochastic source using phaseless data. In practice, the convenient and cheap instrument can only measure the second moment of the random field values, which is the expectation of the total energy and can be calculated using the corresponding expansion coefficients. Without the phase information of the scattering data, our preliminary numerical tests show that a straightforward extension of the hybrid method gives a large reconstruction error. Another interesting and even more challenging problem is to solve the inverse random medium problem. In that case, the medium is no longer deterministic and its uncertainty has to be modeled as well. It is a longer term research and will require new techniques. We hope to be able to address these issues and report the progress elsewhere in the future.

Acknowledgments

The research of GB was supported in part by the NSF grants DMS-0604790, DMS-0908325, CCF-0830161, EAR-0724527, DMS-0968360, and the ONR grant N00014-09-1-0384.

The research of PL was supported in part by the NSF grants DMS-0914595 and EAR-0724656. The research of HZ was supported in part by Faculty Early Career Development (CAREER) Award DMS-0645266.

References

[1] Amundsen L, Reitan A, Helgesen H and Arntsen B 2005 Data-driven inversion/depth imaging derived from approximation to one-dimensional inverse acoustic scattering *Inverse Problems* **21** 1823–50
[2] Badieirostami M, Adibi A, Zhou H and Chow S 2007 Model for efficient simulation of spatially incoherent light using the Wiener chaos expansion method *Opt. Lett.* **32** 3188–90
[3] Bao G, Chow S-N, Li P and Zhou H 2010 An inverse random source problem for the Helmholtz equation, preprint
[4] Bao G, Hou S and Li P 2007 Inverse scattering by a continuation method with initial guesses from a direct imaging algorithm *J. Comput. Phys.* **227** 755–62
[5] Bao G, Hou S and Li P 2007 Recent studies on inverse medium scattering problems *Modeling and Computations in Electromagnetics (Lecture Notes in Computational Science and Engineering* vol 59*)* (Berlin: Springer) pp 165–86
[6] Bao G and Li P 2004 Inverse medium scattering for three-dimensional time harmonic Maxwell equations *Inverse Problems* **20** L1–7
[7] Bao G and Li P 2005 Inverse medium scattering for the Helmholtz equation at fixed frequency *Inverse Problems* **21** 1621–44
[8] Bao G and Li P 2005 Inverse medium scattering problems for electromagnetic waves *SIAM J. Appl. Math.* **65** 2049–66
[9] Bao G and Li P 2007 Inverse medium scattering problems in near-field optics *J. Comput. Math.* **25** 252–65
[10] Bao G and Li P 2007 Numerical solution of inverse scattering for near-field optics *Opt. Lett.* **32** 1465–7
[11] Bao G and Li P 2009 Numerical solution of an inverse medium scattering problem for Maxwell's equations at fixed frequency *J. Comput. Phys.* **228** 4638–48
[12] Bao G and Liu J 2003 Numerical solution of inverse problems with multi-experimental limited aperture data *SIAM J. Sci. Comput.* **25** 1102–17
[13] Bao G and Triki F 2010 Error estimates for the recursive linearization for solving inverse medium problems *J. Comput. Math.* to appear
[14] Bao G and Wu H 2005 Convergence analysis of the perfectly matched layer problems for time-harmonic Maxwell's equations *SIAM J. Numer. Anal.* **43** 2121–43
[15] Berenger J-P 1994 A perfectly matched layer for the absorption of electromagnetic waves *J. Comput. Phys.* **114** 185–200
[16] Berenger J-P 1996 Three-dimensional perfectly matched layer for the absorption of electromagnetic waves *J. Comput. Phys.* **127** 363–79
[17] Bramble J and Pasciak J 2007 Analysis of a finite PML approximation for the three dimensional time-harmonic Maxwell's and acoustic scattering problems *Math. Comput.* **76** 597–614
[18] Cameron R and Martin W 1947 The orthonormal development of non-linear functionals in series of Fourier–Hermite functionals *Ann. Math.* **48** 385–92
[19] Carney P and Schotland J 2003 Near-field tomography *MSRI Ser. Math. Appl.* **47** 131–66
[20] Chen Y 1997 Inverse scattering via Heisenberg's uncertainty principle *Inverse Problems* **13** 253–82
[21] Chen Y 1997 Inverse scattering via skin effect *Inverse Problems* **13** 647–67
[22] Chew W and Wang Y 1990 Reconstruction of two-dimensional permittivity distribution using the distorted Born iteration method *IEEE Trans. Med. Imaging* **9** 218–25
[23] Chen Z and Liu X 2005 An adaptive perfectly matched layer technique for time-harmonic scattering problems *SIAM J. Numer. Anal.* **43** 645–71
[24] Chen Z and Wu X 2008 An adaptive uniaxial perfectly matched layer method for time-harmonic scattering problems *Numer. Math. Theory Methods Appl.* **1** 113–37
[25] Chow P-L 1975 Perturbation methods in stochastic wave propagation *SIAM Rev.* **17** 57–80
[26] Coifman R, Goldberg M, Hrycak T, Israeli M and Rokhlin V 1999 An improved operator expansion algorithm for direct and inverse scattering computations *Waves Random Media* **9** 441–57
[27] Collino F and Monk P 1998 Optimizing the perfectly matched layer *Comput. Methods Appl. Mech. Eng.* **164** 157–71
[28] Colton D, Coyle J and Monk P 2000 Recent development in inverse acoustic scattering theory *SIAM Rev.* **42** 369–414

[29] Colton D and Kress R 1983 *Integral Equation Methods in Scattering Theory* (New York: Wiley)
[30] Colton D and Kress R 1998 *Inverse Acoustic and Electromagnetic Scattering Theory* (*Appl. Math. Sci.* vol 93) 2nd edn (Berlin: Springer)
[31] Courjon D 2003 *Near-Field Microscopy and Near-Field Optics* (London: Imperial College Press)
[32] Devaney A 1979 The inverse problem for random sources *J. Math. Phys.* **20** 1687–91
[33] Dorn O, Bertete-Aguirre H, Berrymann J G and Papanicolaou G C 1999 A nonlinear inversion method for 3D electromagnetic imaging using adjoint fields *Inverse Problems* **15** 1523–58
[34] Engl H, Hanke M and Neubauer A 1996 *Regularization of Inverse Problems* (Dordrecht: Kluwer)
[35] Gelfand I M and Levitan B M 1955 On the determination of a differential equation from its spectral functions *Am. Math. Soc. Transl. Ser. 2* **1** 253–304
[36] Hohage T 2001 On the numerical solution of a three-dimensional inverse medium scattering problem *Inverse Problems* **17** 1743–63
[37] Hohage T 2006 Fast numerical solution of the electromagnetic medium scattering problem and applications to the inverse problem *J. Comput. Phys.* **214** 224–38
[38] Hou T, Luo W, Rozovskii B and Zhou H 2006 Wiener chaos expansions and numerical solutions of randomly forced equations of fluid mechanics *J. Comput. Phys.* **216** 687–706
[39] Ishimaru A 1978 *Wave Propagation and Scattering in Random Media* (New York: Academic)
[40] Keller J B 1962 Wave propagation in random media *Proc. Sympos. Appl. Math.* vol 13 (Providence, RI: American Mathematical Society) pp 227–46
[41] Lassas M and Somersalo E 1998 On the existence and convergence of the solution of PML equations *Computing* **60** 229–41
[42] Natterer F 1986 *The Mathematics of Computerized Tomography* (Stuttgart: Teubner)
[43] Natterer F and Wübbeling F 1995 A propagation–backpropagation method for ultrasound tomography *Inverse Problems* **11** 1225–32
[44] Natterer F and Wübbeling F 2005 Marching schemes for inverse acoustic scattering problems *Numer. Math.* **100** 697–710
[45] Nédélec J-C 2000 *Acoustic and Electromagnetic Equations: Integral Representations for Harmonic Problems* (New York: Springer)
[46] Papanicolaou G C and Keller J B 1971 Stochastic differential equations with applications to random harmonic oscillators and wave propagation in random media *SIAM J. Appl. Math.* **20** 287–305
[47] Teixera F and Chew W 1997 Systematic derivation of anisotropic PML absorbing media in cylindrical and spherical coordinates *IEEE Microw. Guid. Wave Lett.* **7** 371–3
[48] Turkel E and Yefet A 1998 Absorbing PML boundary layers for wave-like equations *Appl. Numer. Math.* **27** 533–57
[49] Vögeler M 2003 Reconstruction of the three-dimensional refractive index in electromagnetic scattering by using a propagating-backpropagation method *Inverse Problems* **19** 739–53
[50] Weglein A, Araújo F, Carvalho P, Stolt R, Matson K, Coates R, Corrigan D, Foster D, Shaw S and Zhang H 2003 Inverse scattering series and seismic exploration *Inverse Problems* **19** R27–83
[51] Xiu D and Karniadakis G 2002 The Wiener-Askey polynomial chaos for stochastic differential equations *SIAM J. Sci. Comput.* **24** 619–44
[52] Yuste R 2005 Fluorescence microscopy today *Nature Methods* **2** 902–4